Article

Single Polymer Chains as Specific Transducers of Molecular Recognition in Scanning Probe Microscopy

Rachel Gabai, Lior Segev, and Ernesto Joselevich

J. Am. Chem. Soc., **2005**, 127 (32), 11390-11398• DOI: 10.1021/ja051642v • Publication Date (Web): 27 July 2005

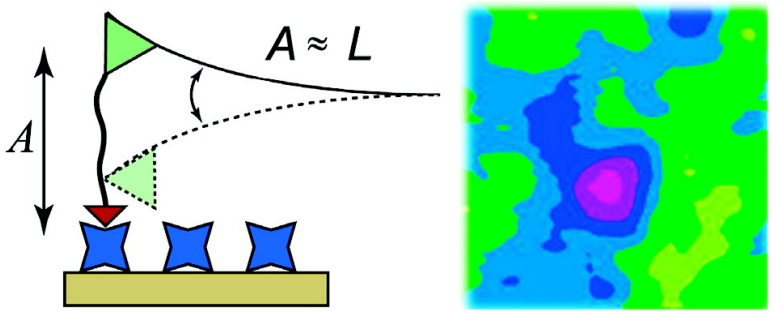

More About This Article

Additional resources and features associated with this article are available within the HTML version:

- Supporting Information
- Links to the 3 articles that cite this article, as of the time of this article download
- Access to high resolution figures
- Links to articles and content related to this article
- Copyright permission to reproduce figures and/or text from this article

View the Full Text HTML

J|A|C|S
ARTICLES
Published on Web 07/27/2005

Single Polymer Chains as Specific Transducers of Molecular Recognition in Scanning Probe Microscopy

Rachel Gabai, Lior Segev, and Ernesto Joselevich*

Contribution from the Department of Materials and Interfaces, Weizmann Institute of Science, Rehovot 76100, Israel

Received March 15, 2005; E-mail: ernesto.joselevich@weizmann.ac.il

Abstract: A new approach for the specific detection and mapping of single molecule recognition is presented, based on the nonlinear elastic behavior of a single polymer chain. The process of molecular recognition between a ligand and a receptor is inherently accompanied by a decrease in the translational and rotational degrees of freedom of the two molecules. We show that a polymeric tether linked to the ligand can effectively transduce the configurational constraint imposed by molecular recognition into a measurable force, which is dominated by the entropic elasticity of the polymer. This force is specifically characterized by a strong nonlinearity when the extension of the polymer approaches its contour length. Thus, a polymer chain tethering the ligand to an oscillating cantilevered tip gives rise to a highly anharmonic motion upon ligand−receptor binding. Higher-harmonics atomic force microscopy allows us to detect this phenomenon in real time as a specific signature for the probing and mapping of single-molecule recognition.

Introduction

The development of single-molecule devices is a current topic of intensive research.[1] Much emphasis has been given to the development of single-molecule *electronic* devices,[2] while there is also a growing interest in the investigation of single-molecule *mechanical* devices, including electromechanical[3] and optomechanical[4] single-molecule devices. Mechanical transducers of single molecule recognition are of particular interest as chemical and biological sensors.[5] During the last two decades, significant advances in physics, chemistry, and biology have been enabled by the development of a series of proximal probes capable of locally addressing, measuring, and mapping different physical phenomena at the single-molecule or nanometer scale, such as electron tunneling,[6] atomic forces,[7] near-field optical absorption or emission,[8] electrochemical currents,[9] and other phenomena that constitute the basis for a variety of scanning probe microscopies.[10] Molecular recognition, namely the highly specific binding between single molecules, is one of the most fundamental molecular processes in biological systems. Molecular recognition probes based on fluorescence have already become essential research tools in molecular and cell biology, as well as the basis for a vast range of protocols in medical diagnosis and biotechnology. Single-molecule spectroscopy of these probes is becoming widely used for the study of biological systems.[11] Isotopic and spin-labeled molecular probes are also widely used in biological nuclear magnetic resonance and electron-spin resonance, respectively. However, all these nonproximal probes must usually be addressed from a long distance via some form of radiation. This has the advantage of nonin-

(1) (a) Joachim, C.; Gimzewski, J. K.; Aviram, A. *Nature* **2000**, *408*, 541−548. (b) Wassel, R. A.; Gorman, C. B. *Angew. Chem., Int. Ed.* **2004**, *43*, 5120−5123.
(2) (a) Kubatkin, S.; Danilov, A.; Hjort, M.; Cornil, J.; Brédas, J. L.; Stuhr-Hansen, N.; Hedegård, P.; Bjørnholm, T. *Nature* **2003**, *425*, 698−701. (b) Tans, S. J.; Verschueren, A. R. M.; Dekker, C. *Nature* **1998**, *393*, 49−52. (c) Liang, W. J.; Shores, M. P.; Bockrath, M.; Long, J. R.; Park, H. *Nature* **2002**, *417*, 725−729. (d) Park, J.; Pasupathy, A. N.; Goldsmith, J. I.; Chang, C.; Yaish, Y.; Petta, J. R.; Rinkoski, M.; Sethna, J. P.; Abruña, H. D.; McEuen, P. L.; Ralph, D. C. *Nature* **2002**, *417*, 722−725. (e) Bumm, L. A.; Arnold, J. J.; Cygan, M. T.; Dunbar, T. D.; Burgin, T. P.; Jones, L.; Allara, D. L.; Tour, J. M.; Weiss, P. S. *Science* **1996**, *271*, 1705−1707. (f) Reed, M. A.; Zhou, C.; Muller, C. J.; Burgin, T. P.; Tour, J. M. *Science* **1997**, *278*, 252−254. (g) Donhauser, Z. J.; Mantooth, B. A.; Kelly, K. F.; Bumm, L. A.; Monnell, J. D.; Stapleton, J. J.; Price, D. W.; Rawlett, A. M.; Allara, D. L.; Tour, J. M.; Weiss, P. S. *Science* **2001**, *292*, 2303−2307. (h) Lewis, P. A.; Inman, C. E.; Yao, Y. X.; Tour, J. M.; Hutchison, J. E.; Weiss, P. S. *J. Am. Chem. Soc.* **2004**, *126*, 12214−12215.
(3) (a) Xu, B. Q.; Xiao, X. Y.; Tao, N. J. *J. Am. Chem. Soc.* **2003**, *125*, 16164−16165. (b) Collier, C. P.; Jeppesen, J. O.; Luo, Y.; Perkins, J.; Wong, E. W.; Heath, J. R.; Stoddart, J. F. *J. Am. Chem. Soc* **2001**, *123*, 12632−12641. (c) Flood, A. H.; Peters, A. J.; Vignon, S. A.; Steuerman, D. W.; Tseng, H. R.; Kang, S.; Heath, J. R.; Stoddart, J. F. *Chem. Eur. J.* **2004**, *10*, 6558−6564. (d) Park, H.; Park, J.; Lim, A. K. L.; Anderson, E. H.; Alivisatos, A. P.; McEuen, P. L. *Nature* **2000**, *407*, 57−60. (e) Sazonova, V.; Yaish, Y.; Ustunel, H.; Roundy, D.; Arias, T. A.; McEuen, P. L. *Nature* **2004**, *431*, 284−287.
(4) Hugel, T.; Holland, N. B.; Cattani, A.; Moroder, L.; Seitz, M.; Gaub, H. E. *Science* **2002**, *296*, 1103−1106.
(5) (a) Albrecht, C.; Blank, K.; Lalic-Multhaler, M.; Hirler, S.; Mai, T.; Gilbert, I.; Schiffmann, S.; Bayer, T.; Clausen-Schaumann, H.; Gaub, H. E. *Science* **2003**, *301*, 367−370. (b) Stroh C.; Wang, H.; Bash, R.; Ashcroft, B.; Nelson, J. Gruber, H.; Lohr, D.; Lindsay, S. M.; Hinterdorfer, P. *Proc. Natl. Acad. Sci. U.S.A.* **2004**, *101*, 12503−12507.
(6) (a) Binnig, G.; Roher, H.; Gerber, C.; Weibel, E. *Appl. Phys. Lett.* **1982**, *40*, 178−180. (b) Binnig, G.; Roher, H.; Gerber, C.; Weibel, E. *Phys. Rev. Lett.* **1982**, *49*, 57−61.
(7) (a) Binnig, G.; Quate, C. F.; Gerber, C. *Phys. Rev. Lett.* **1986**, *56*, 930−933. (b) Drake, B.; Prater, C. B.; Weisenhorn, A. L.; Gould, S. A.; Albrecht, T. R.; Quate C. F.; Cannell, D. S.; Hansma, H. G.; Hansma, P. K. *Science* **1989**, *243*, 1586−1589.
(8) (a) Betzig, E.; Lewis, A.; Harootunian, A.; Isaacson, M.; Kratschmer, E. *Biophys. J.* **1986**, *49*, 269−279. (b) Betzig, E.; Chichester, R. J. *Science* **1993**, *262*, 1422−1425.
(9) Bard, A. J.; Fan, F. R. F.; Kwak, J.; Lev, O. *Anal. Chem.* **1989**, *61*, 132−138.
(10) (a) Gimzewski, J. K.; Joachim, C. *Science* **1999**, *283*, 1683−1688. (b) Engel, A. *Annu. Rev. Biophys. Biol.* **1991**, *20*, 79−108. (c) Wiesendanger, R. *Scanning Probe Microscopy and Spectroscopy: Methods and Applications* Cambridge University Press: New York, 1994. (d) Bonnell, D. *Scanning Probe Microscopy and Spectroscopy: Theory, Techniques, and Applications*; Wiley-VCH Inc.: New York, 2001.
(11) Nie, S. M.; Zare, R. N. *Annu. Rev. Biophys. Biomol. Struct.* **1997**, *26*, 567−596.

10.1021/ja051642v CCC: $30.25

trusiveness, but the disadvantage of low spatial resolution. Following the current advances in scanning probe microscopy, the development of proximal probes for single-molecule recognition could open up vast possibilities for the characterization of biological systems.

Atomic force microscopy (AFM),[7] which in its various modes has become the most widely used scanning probe microscopy, normally provides a topographic image of samples, which is not specifically sensitive to the chemical functionalities present on the surface. Chemically sensitive imaging, sometimes referred to as chemical force microscopy,[12] has been achieved using chemically functionalized probing tips.[13] Measuring the adhesion,[12a] friction[14] or oscillatory dephasing[15] of these tips with the sample provides a contrast between regions containing different chemical functionalities on the surface, arising from relatively general intermolecular forces,[16] such as hydrophilic/hydrophobic, electrostatic, and hydrogen bonding. High-resolution imaging of surface charge has been obtained by more sophisticated AFM methods, such as higher-harmonic imaging,[17] pulsed force,[18] and lift mode.[19]

Besides these rather general intermolecular and surface interactions, the highly specific interactions between single molecules have been widely studied by AFM as a spectroscopic tool. Single-molecule force spectroscopy,[20] which measures probe−sample forces as a function of probe−sample distance, has provided significant knowledge on the dynamics and energy landscape of ligand−receptor binding,[21] DNA hybridization,[22,5a] antigen−antibody binding,[23] supramolecular assembly,[24] and covalent bonding,[25] as well as on the conformational dynamics and elasticity of DNA,[26] proteins,[27] polysaccharides[28] and a variety of polymers.[29] The specific mapping of these molecular recognition and conformational transition processes, however, remains a significant challenge. Spatial maps of molecular recognition were initially obtained by processing the results of many force−distance hystresis loops performed on an array of points of the surface.[30] The recorded unbinding forces measured in each loop derive from the energy landscape of the ligand−receptor interaction. Since each force−distance measurement is limited by the binding and unbinding time, as well as by the mechanical relaxation of the probe cantilever, this is a time-consuming imaging process and thus subject to thermal drifts and aberrations.

Dynamic force microscopy modes, often referred to also as intermittent contact or tapping mode,[31] have significant advantages for imaging delicate samples in liquid, namely, reduced friction, gentle and short contact, and high feedback stability. On the other hand, some of these features can pose limitations for the imaging of specific binding between molecules at the tip and the sample, namely, a short dwell time compared to that for the molecular binding process, and a shortage of degrees of freedom that are necessary for the molecules to reach each other with the right conformation and orientation. Hinterdorfer and co-workers have overcome some of these limitations and achieved efficient molecular recognition imaging by tethering the probing ligand to the AFM tip through a flexible polymer chain.[32] The images thus obtained show the receptor molecules with a swollen apparent topography that arises from the extension of the tether upon ligand−receptor binding when the peak-to-peak amplitude of the tip oscillations are significantly smaller than the contour length of the tether. Upon addition of excess ligand to the solution while imaging, the receptor sites become blocked, and the increased apparent topography of the receptor molecules converts into real topography. By comparing the images before and after inhibition, one can identify the binding sites on the surface. The topographic image alone, however, does not provide a specific signature of molecular recognition. A proximal probe of molecular recognition that can specifically highlight the molecular recognition itself, independently of topography, is a major challenge in chemical and biological scanning probe microscopy. Recent progress has been made using the DC component of deflection signal,[5b] and the

(12) (a) Frisbie, C. D.; Rosznyai, L. F.; Noy, A.; Wrighton, M. S.; Lieber, C. M. *Science* **1994**, *265*, 2071−2074. (b) Noy, A.; Vezenov, D. V.; Lieber, C. M. *Annu. Rev. Mater. Sci* **1997**, *27*, 381−421. (c) McKendry, R.; Theoclitou, M. E.; Rayment, T.; Abell, C. *Nature* **1998**, *391*, 566−568. (d) Nakagawa, T.; Ogawa, K.; Kurumizawa, T. *J. Vac. Sci. Technol. B* **1994**, *12*, 2215−2218.

(13) (a) Vezenov, D. V.; Noy, A.; Rosznyai, L. F.; Lieber, C. M. *J. Am. Chem. Soc.* **1997**, *119*, 2006−2015. (b) van der Vegte, E. W.; Hadziioannou, G. *Langmuir* **1997**, *13*, 4357−4368. (c) Knapp, H. F.; Wiegrabe, W.; Heim, M.; Eschrich, R.; Guckenberger, R. *Biophys. J.* **1995**, *69*, 708−715. (d) Wong, S. S.; Woolley, A. T.; Joselevich, E.; Cheung, C. L.; Lieber, C. M. *J. Am. Chem. Soc.* **1998**, *120*, 8557−8558. (e) Ito, T.; Namba, M.; Buhlmann, P.; Umezawa, Y. *Langmuir* **1997**, *13*, 4323−4332. (f) Alley, R. L.; Komvopoulos, K.; Howe, R. T. *J. Appl. Phys*. **1994**, *76*, 5731−5737.

(14) (a) Noy, A.; Frisbie, C. D.; Rosznyai, L. F.; Wrighton, M. S.; Lieber, C. M. *J. Am. Chem. Soc.* **1995**, *117*, 7943−7951. (b) Green, J. B. D.; Mcdermott, M. T.; Porter, M. D.; Siperko, L. M. *J. Phys. Chem.* **1995**, *99*, 10960−10965.

(15) (a) Noy, A.; Sanders, C. H.; Vezenov, D. V.; Wong, S. S.; Lieber, C. M. *Langmuir* **1998**, *14*, 1508−1511. (b) Cleveland, J. P.; Anczylowski, B.; Schmid, A. E.; Elings, V. B. *Appl. Phys. Lett.* **1998**, *72*, 2613−2615.

(16) Israelachvili, J. *Intermolecular and Surface Forces*, 2nd ed.; Academic Press: New York, 1991.

(17) van Noort, S. J. T.; Willemsen, O. H.; van der Werf, K. O.; de Grooth, B. G.; Greve, J. *Langmuir* **1999**, *15*, 7101−7107.

(18) (a) Schneider, M.; Zhu, M.; Papastavrou, G.; Akari, S.; Mohwald, H. *Langmuir* **2002**, *18*, 602−606. (b) Krotil, H. U.; Stifter, T.; Waschipky, H.; Weishaupt, K.; Hild, S.; Marti, O. *Surf. Interface Anal.* **1999**, *27*, 336−340. (c) Miyatani, T.; Horii, M.; Rosa, A.; Fujihira, M.; Marti, O. *Appl. Phys. Lett.* **1997**, *71*, 2632−2634. (d) Krüger, S.; Krüger, D.; Janshoff, A. *ChemPhysChem* **2004**, *5*, 989−997. (e) Okabe, Y.; Akiba, U.; Fujihira, M. *Appl. Surf. Sci*. **2000**, *157*, 398−404.

(19) Johnson, A. S.; Nehl, C. L.; Mason, M. G.; Hafner, J. H. *Langmuir* **2003**, *19*, 10007−10010.

(20) Fisher, T. E.; Marszalek P. E.; Fernandez J. M. *Nat. Struct. Biol.* **2000**, *7*, 719−724.

(21) (a) Merkel, R.; Nassoy, P.; Leung, A.; Ritchie, K.; Evans, E. *Nature* **1999**, *397*, 50−53. (b) Nevo, R.; Stroh, C.; Kienberger, F.; Kaftan, D.; Brumfeld, V.; Elbaum, M.; Reich, Z.; Hinterdorfer, P. *Nat. Struct. Biol.* **2003**, *10*, 553−557.

(22) (a) Rief, M.; Clausen-Schaumann, H.; Gaub, H. *Nat. Struct. Biol.* **1999**, *6*, 346−349. (b) Oroszlan, T. S. K.; Schäfer, R.; Güntherodt, H.-J. *Proc. Natl. Acad. Sci. U.S.A.* **1999** *96*, 11277−11282.

(23) (a) Hinterdorfer, P.; Baumgartner, W.; Gruber, H. J.; Schilcher, K.; Schindler, H. *Proc. Natl. Acad. Sci. U.S.A.* **1996**, *93*, 3477−3481. (b) Ros, R.; Schweisinger, F.; Anselmetti, D.; Kubon, M.; Schäfer, R.; Plückthun, A.; Tiefenauer, L. *Proc. Natl. Acad. Sci. U.S.A.* **1998**, *95*, 7402−7405.

(24) (a) Skulason, H.; Frisbie, C. D. *J. Am. Chem. Soc.* **2002**, *124*, 15125−15133. (b) Auletta, T.; de Jong, M. R.; Mulder, A.; van Veggel, F. C. J. M.; Huskens, J.; Reinhoudt, D. N.; Zou, S.; Zapotoczny, S.; Schonherr, H.; Vancso, G. J.; Kuipers, L. *J. Am. Chem. Soc.* **2004**, *126*, 1577−1584. (c) Schoenherr, H.; Beulen, M. J.; Buegler, J.; Huskerns, J.; Van Veggel, F. C. J. M.; Reinhoudt, D. N.; Vancso, F. J. *J. Am.* Chem. Soc. **2000**, *122*, 4963−4967.

(25) Grandbois, M.; Beyer, M.; Rief, M.; Clausen-Schaumann, H.; Gaub, H. E. *Science* **1999**, *283*, 1727−1730.

(26) (a) Noy, A.; Vezenov, D. V.; Kayyem, J. F.; Meade, T. J.; Lieber, C. M. *Chem. Biol.* **1997**, *4*, 519−527. (b) Clausen-Schaumann, H.; Rief, M.; Tolksdorf, C.; Gaub, H. E. *Biophys. J.* **2000**, *78*, 1997−2007.

(27) Rief, M.; Gautel, M.; Oesterhelt, F.; Fernandez, J. M.; Gaub, H. E *Science* **1997**, *276*, 1109−1112.

(28) (a) Rief, M.; Oesterhelt, F.; Heymann, B.; Gaub, H. E. *Science* **1997**, *275*, 1295−1297. (b) Marszalek, P. E.; Oberhauser, A. F.; Pang, Y. P.; Fernandez, J. M. *Nature* **1998**, *396*, 661−664.

(29) (a) Oesterhelt, F.; Rief, M.; Gaub, H. *New J. Phys.* **1999**, 6.1−6.11. (b) Shi, W. Q.; Cui, S. X.; Wang, C.; Wang, L.; Zhang, X.; Wang, X. J.; Wang, L. *Macromolecules* **2004**, *37*, 1839−1842.

(30) Hinterdorfer, P.; Baumgartner, W.; Gruber, H. J.; Schilcher, K.; Schindler, H. *Proc. Natl. Acad. Sci. U.S.A.* **1996**, *93*, 3477−3481.

(31) Giles, R.; Cleveland, J. P.; Manne, S.; Hansma, P. K.; Drake, B.; Maivald, P.; Boles, C.; Gurley, J.; Elings, V. *Appl. Phys. Lett.* **1993**, *63*, 617−618.

(32) Raab, A.; Han, W.; Badt, D.; Smith-Gill, S. J.; Lindsay, S. M.; Schindler, H.; Hinterdrfer, P. *Nat. Biotechnol.* **1999**, *17*, 901−905.

upper value of the cantilever deflection,[33] as indicative of molecular recognition. These methods, however, do not exploit the unique elastic properties of the polymer tether to gain specificity for the imaging of molecular recognition.

Here we present a new approach for the specific detection and mapping of molecular recognition based on the nonlinear elastic properties of a polymer tether. This approach allows us not only to overcome the problem of degrees of freedom mentioned before but also to actually exploit it for the highly specific detection of molecular recognition at the single-molecule level, simultaneously and independently of topography. A process of molecular recognition between two molecules is inherently accompanied by a decrease in their translational and rotational degrees of freedom. We find that a polymeric tether can effectively transduce the configurational constraint imposed by molecular recognition into a measurable force. This force, which is dominated by the entropic elasticity of the polymer, is specifically characterized by a strong nonlinearity, which gives rise to highly anharmonic oscillations of the probe cantilever upon molecular recognition. Higher-harmonics imaging in tapping mode AFM (HH-AFM)[34] at an amplitude near the contour length of the tether allows us to detect this phenomenon in real time as a specific signature for the probing and mapping of single-molecule recognition.

Experimental Section

Materials. NaCl (BioLab Ltd., Israel), KCl (Merck), sodium dihydrogen phosphate monohydrate (Merck), ethanol (Baker), DMSO (Merck), dry toluene (Merck), 16-mercaptohexadecanoic acid (Aldrich), 3-(aminopropyl)triethoxisilane (Aldrich), 1-ethyl-3-(3-dimethylaminopropyl)carbodiimide hydrochloride (EDC) (Pierce), *N*-hydroxysulfosuccinimide (Pierce), streptavidin (Pierce), poly(ethylene glycol)-α-biotin-ω-NHS-ester MW 3400 (Shearwater), and D-biotin (Sigma) were available commercially and used as received. Silicon wafers of (100) orientation were obtained from International Wafer Service, Inc. Standard V-shaped Si_3N_4 AFM cantilevers (100 μm narrow or 200 μm narrow) with pyramidal tips were obtained from Digital Instrument, Santa Barbara, CA. All water was deionized with a Millipore (Simplicity 185) to 18 MΩ·cm resistivity.

Sample Preparation. Si (100) substrates were coated with a 20-nm adhesion layer of Cr followed by 50 nm of Au, using an electron-beam evaporator at deposition rate of 0.2 and 0.05 nm/s, respectively, on a liquid-N_2-cooled sample stage. The samples were first coated with carboxylic group by immersion in a 1 mM ethanol solution of 16-mercaptohexadecanoic acid for at least 12 h, and then immersion in 15 mM sulfo-NHS and 75 mM EDC in pH 6.0 phosphate buffer saline (PBS) (10 mM phosphate buffer, 6 mM KCl, 120 mM NaCl) for 1 h, to assist carbodiimide coupling. After washing with buffer and water, and drying with a flowing stream of N_2, the samples were placed in a solution of 0.2 g/L of streptavidin in the PBS buffer for 2 h, to covalently couple the protein to the surface. After being rinsed with buffer without drying, the samples were ready to use. By using this procedure, the streptavidin was covalently bound to the surface. Addition of free biotin to a solution did not lead to detachment of streptavidin molecules.

Probe Preparation. Functionalized silicon nitride cantilevered tips with a 35-nm-long poly(ethylene glycol) (PEG) chain ending with a biotin group were prepared by first silanizing the tips in a 2% solution of aminopropyltriethoxisilane in toluene, and then incubating in a 1 mM solution of the biotin-PEG-NHS in DMSO. After rinsing with the solvent and drying under a stream of nitrogen, the tips were ready to use. The spring constant of each tip was determined in air by a standard thermal noise method (vide infra).[35]

Experimental Setup and Measurement Conditions. Topographic, as well as higher-harmonics atomic force microscopy (HH-AFM) and spectroscopy measurements were made with a commercial AFM (Veeco, Nanoscope IV, Multi-Mode) equipped with a fluid cell, coupled to a lock-in-amplifier with fast harmonic analysis capability (Perkin-Elmer, DSP-7280). The signal corresponding to the amplitude of the specific harmonic under study is obtained by feeding the AFM photodetector signal into the lock-in amplifier, using the AFM drive signal as a lock-in reference. The lock-in output signal corresponding to the specified higher harmonic amplitude is fed into the AFM controller. HH-AFM images were obtained simultaneously with topographic images, by performing the usual liquid tapping mode imaging, which uses the tip oscillation amplitude as a feedback signal, while measuring the specific harmonic amplitude signal as a function of *x*,*y* tip position. Higher-harmonics (HH) force spectroscopy measurements were done simultaneously with force measurements by approaching and retracting the sample (at 0.5 Hz) to the oscillating tip and then measuring the specific harmonic amplitude signal as a function of *z*-piezo extension. In all measurements, the tips were driven at their resonance frequency in liquid (8−9 and 20−25 kHz for 200 and 100 μm-long cantilevers, respectively), which was independently determined by recording the noise spectrum in liquid with a spectrum analyzer (Stanford Research Systems SR760). The spring constants of the cantilevers were measured by the same thermal noise method, but in air, and were found to be 0.005−0.12 and 0.1−0.3 N/m for 200 and 100 μm-long cantilevers, respectively. For HH-AFM imaging, the lock-in acquisition time was 500 μs, which is at least 10 times larger than oscillation period, and at least 8 times smaller than the dwell time per pixel at 512 × 512 resolution. The phase of higher harmonics was zeroed prior to the acquisition of each image. Phase changes were usually small so that, after zeroing the phase, there was no significant difference between the in-phase signal (lock-in "*X*" output) and the modulus signal ("*R*" output = $(X^2 + Y^2)^{1/2}$). This allows us to correctly interpret the recorded in-phase signal as the amplitude of higher harmonics.

The oscillatory motion of the probes was simply monitored by feeding the AFM photodetector signal to a LabView-controlled data acquisition card (National Instruments 5112) in a PC computer, using the AFM drive piezo signal as an external trigger.

Approach and Theory

Specific Probing Mechanism. The molecular recognition probe consists of a single ligand tethered by a polymer chain to the apex of an AFM tip. The tether confers to the ligand a large number of degrees of freedom, which allow it to explore all its possible configurations while scanning, until a molecular recognition event takes place. After the molecular recognition event occurs, the polymer chain loses part of its configurational entropy and will try to regain it by pulling from the other end. The tension along the polymer chain will be equal to the extension-derivative of its free energy, the main component of which is the entropic term.

The performance of the specific molecular recognition probe in tapping mode can be rationalized by describing its behavior in three different regimes of amplitude with respect to the contour length of the tether, as schematically represented in Figure 1a. (a) When the peak-to-peak amplitude of the tip

(33) Stroh, C. M.; Ebner, A.; Geretschlager, M.; Freudenthaler, G.; Kienberger, F.; Kamruzzahan, A. S. M.; Smith-Gil, S. J.; Gruber, H. J.; Hinterdorfer, P. *Biophys. J.* **2004**, *87*, 1981−1990.

(34) (a) Stark, M.; Stark, R. W.; Heckl, W. M.; Guckenberger, R. *Proc. Natl. Acad. Sci. U.S.A.* **2002**, *99*, 8473−8478. (b) Stark, R. W.; Heckl, W. M. *Rev. Sci. Instr.* **2003**, *74*, 5111−5114.

(35) Hutter, J. L.; Bechhoefer, J. *Rev. Sci. Instrum.* **1993**, *64*, 1868−1873.

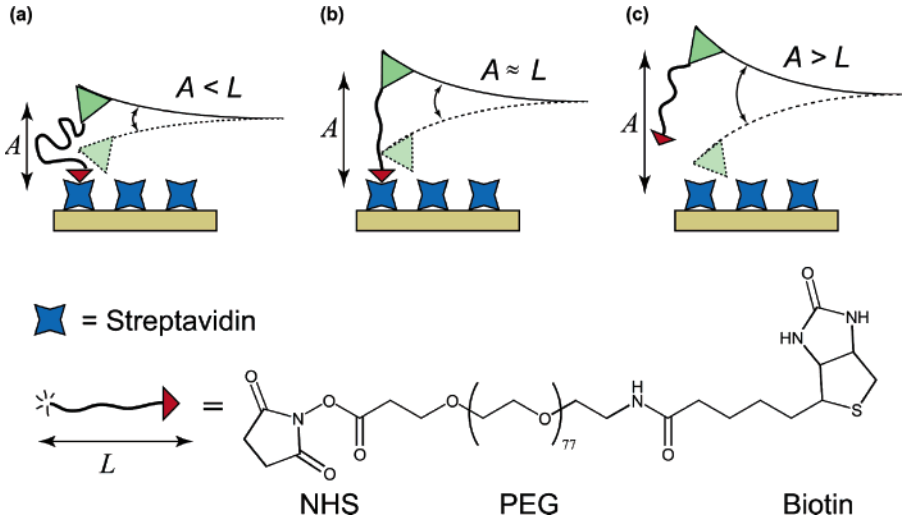

Figure 1. Schematic representation of the performance of a specific probe consisting of a ligand tethered to an AFM tip by a polymer chain, at three different regimes of peak-to-peak amplitude (A) relative to the contour length of the tether (L). (a) A a fraction of L. (b) A comparable to L. (c) A larger than L.

oscillation A, which is maintained by the feedback system, is only a fraction of the length of the tether L (Figure 1a), then the ligand can reach a receptor lying on the surface below the tip and a binding event can occur without interruption. In this regime, the entropic elasticity of the polymer is relatively low, and the forces acting on the cantilever are dominated by its linear (i.e. Hookean) restoring force plus short-range, nonspecific tip−sample interactions. Then, the cantilever motion is relatively harmonic as in usual dynamic force microscopy.[36] (b) When the peak-to-peak amplitude approaches the tether length (Figure 1b), the entropic elasticity of the polymer chain significantly contributes to the restoring force. Since this force is acutely nonlinear over a significant range, the Hookean approximation no longer holds, and the cantilever motion becomes anharmonic. (c) When the peak-to-peak amplitude is larger than the tether length (Figure 1c), the dwell time of the ligand near the receptor is too short to allow for continuous binding, and the cantilever motion is again harmonic, as in regime (a).

Nonlinear Dynamics of the Probe. Theoretical models of dynamic force microscopy in liquid have been widely reported in the literature.[36−38] The cantilever dynamics and motion are usually described by an equation of motion that compensates all the conservative, dissipative, inertial, and driving forces acting on the cantilever. In our case, the equation of motion can be written as eq 1,

$$m\frac{\partial^2 z}{\partial t^2} + \gamma\frac{\partial z}{\partial t} + kz + F_{ts}(d) + F(d) = F_0 \sin(2\pi\nu t) \quad (1)$$

where z is the cantilever deflection, or the tip position with respect to that of cantilever equilibrium, m is the effective reduced mass of the cantilever, γ is the friction coefficient due to solvent viscosity or any other dissipative processes, k is the cantilever spring constant, F_{ts} is the nonspecific tip−sample interaction force, which is a function of the tip−sample distance d, F is the interaction force of the probe, including the polymer and the ligand−receptor binding, and $F_0 \sin(2\pi\nu t)$ is the sinusoidal driving force generated by the piezo drive at frequency ν. The tip−sample distance d is related to the cantilever deflection z and the z-piezo displacement from contact position, z_0, as given by eq 2.

$$d = z + z_0 \quad (2)$$

Nonspecific tip−sample interactions have been described in the framework of Derjaguin−Landau−Verwey−Overbeek (DLVO) theory,[16] considering electrostatic double layer and van der Waals interactions. At sufficiently high ionic strengths, the Debye length becomes short enough for electrostatic forces to be neglected, so that nonspecific tip−sample forces can be approximated as van der Waals forces between a sphere and a flat surface,[39] including the Born repulsion, as given by eq 3,

$$F_{ts}(d) = \frac{HR}{3}\left(\frac{1}{d^2} - \frac{r_0^6}{d^8}\right) \quad (3)$$

where H is the Hamaker constant, R is the radius of a sphere representing the tip, and r_0 is the smallest separation between the tip and the sample that follow the Pauli exclusion force.

The probe force F includes the polymer elasticity and the ligand−receptor interaction. The latter is very stiff and short-ranged compared to the former, so that, in terms of motion, the overall probe force can be approximated as the pure polymer elasticity ending with a sharp drop beyond the ligand−receptor unbinding force. Such interaction between tethered ligand−receptor assemblies and the interesting way in which the tether affects the ligand−receptor interactions have been well characterized by surface force apparatus (SFA) measurements.[40] The elasticity of single polymer chains of poly(ethylene glycol) (PEG) in aqueous solution, on the other hand, has been characterized by force spectroscopy.[29a] The results were well described by three contributions leading to three force-extension regimes: first the entropic elasticity, then a transition from hydrogen-bonding-stabilized gauche conformation to the more

(36) Garcia, R.; Perez, R. *Surf. Sci. Rep.* **2002**, *47*, 197−301.
(37) Tamayo, J.; Garcia, R. *Langmuir* **1996**, *12*, 4430−4435.
(38) Tamayo, J.; Garcia, R. *Appl. Phys. Lett.* **1997**, *71*, 2394−2396.
(39) Willemsen, O. H.; Snel, M. M. E.; Kuipers, L.; Figdor, C. G.; Greve, J.; de Grooth, B. G. *Biophys. J.* **1999**, *76*, 716−724.
(40) Wong, J. Y.; Kuhl, T. L.; Israelachvili, J. N.; Mullah, N.; Zalipsky, S. *Science* **1997**, *275*, 820−822.

extended trans conformation, and finally the segment elasticity of the polymer. Equation 4 describes the extension of PEG in water as a function of the end-to-end force,

$$d(F) = N_s\left(\frac{L_{trans}}{1+e^{-\Delta G/k_BT}} + \frac{L_{gauche}}{1+e^{+\Delta G/k_BT}}\right) \times \left[\coth\left(\frac{Fl_K}{k_BT}\right) - \frac{k_BT}{Fl_K}\right] + N_s\frac{F}{K_s} \quad (4)$$

where d is the extension of the tether, F is the force, l_K is the Kuhn length (the length of the statistically independent segments), L is the contour length (the fully extended length of the relaxed tether), N_s is the number of segments (monomers) and K_s is the segment elasticity (spring constant per monomer), k_B is the Boltzmann constant, T is the temperature, L_{trans} and L_{gauche} are the monomer lengths in the trans and gauche conformations, respectively, and ΔG is the free energy difference of the conformational transition as a function of the force. $\Delta G(F)$ is given by eq 5, where G_{trans} and G_{gauche} are the free energies per monomer in the trans and gauche conformations, respectively.

$$\Delta G(F) = (G_{trans} - G_{gauche}) - F\,(L_{trans} - L_{gauche}) \quad (5)$$

When the tip and probe oscillate far from the surface, the terms F_{ts} and F in the equation of motion (eq 1) are zero, and the oscillation is approximately that of a damped harmonic oscillator. When the tip approaches the sample, the term F_{ts} takes effect, leading to the usual reduction in amplitude that is kept constant by the feedback system in the repulsive regime of tapping mode AFM. The nonlinear F_{ts} term introduces a deviation from harmonic motion, but this is minimized as the setpoint amplitude is set close to the free amplitude far from the surface. Upon molecular recognition, the long-range, nonlinear term F adds on to the equation of motion, leading to a pronounced deviation from harmonic oscillation. As a first approximation, we neglect the viscous response of the tether that could be added to that of the cantilever, tip, sample, and solvent, so that γ is held constant. This approximation may not be fully justified in the case of viscoelastic polymer stretching, which should lead to energy dissipation. However, it allows us to present a workable model that qualitatively reproduces the results to a large extent. Energy dissipation has been recently used for chemical force microscopy imaging[41] but has not yet been tested for a polymer-tethered ligand on a receptor sample. We also assume the equilibrium polymer elasticity (eq 4), even though the oscillation period is shorter than the relaxation time of the polymer.[40] This may be justified by considering that the reduction in the number of possible configurations of the polymer near full extension is more significant than near full relaxation. Therefore, the most significant part of the relaxation, in term of forces, takes place faster than the full relaxation of the polymer. All the parameters in eq 1 can be experimentally estimated or extrapolated, and applied to fit numerical simulations to experimental conditions. These parameters include the experimental resonance frequency and quality factor, which are determined from the thermal noise spectrum recorded in liquid, the spring constant previously determined in air,[35] and the driving force required to obtain a particular free amplitude.

Results and Discussion

Characterization and Selection of Single-Molecule Entropic Probes. The probes, consisting of biotin-PEG-functionalized AFM tips, were first characterized by conventional force spectroscopy on a substrate containing covalently immobilized streptavidin molecules, and then selected according to their characteristics. Only probes containing a single tethered ligand at the apex of the AFM tip were selected. Probes having multiple ligands, or a single one but not at the apex, were discarded (see Supporting Information for force−distance curves and details of the selection process). The detachment or "pull-off" takes place at a distance of ~30 nm from the tip−surface contact position, corresponding to the contour length of the PEG tether, 30 ± 5 nm. The unbinding force was consistent with previously reported values for biotin−streptavidin at the fast loading-rate limit, 200 pN.[42,21a] The success rate of good probes is about 20%. All the probes were remarkably robust and could be used, washed, dried, stored in a box, and reused again and again for tens of experiments and several months, without any detectable deterioration. This sharply contrasts with fluorescent single-molecule probes, which tend to be rapidly bleached by light in the course of experiments.[43]

Higher-Harmonics Force Spectroscopy. The oscillatory motion of the probes, and the effect of molecular recognition, were studied by higher-harmonics force spectroscopy measurements, hereby introduced for the first time, to the best of our knowledge. In these experiments, the probes were approached and retracted from the surface while driving the cantilever into resonance at peak-to-peak amplitudes smaller than the contour length of the polymer. The amplitudes of the first and higher harmonics were monitored in real time as a function of z-piezo displacement. In addition, the actual motion of the cantilever shortly before and after the ligand−receptor unbinding event was directly monitored as a function of time and Fourier-analyzed off-line.

Figure 2 shows the second-harmonics force spectroscopy measurement of the 30-nm-long PEG-biotin molecule at a peak-to-peak amplitude of 9 nm (30% of the contour length) upon biotin−streptavidin binding and unbinding. The interesting features are seen when the sample is retracted from the tip.

The first harmonic amplitude (Figure 2a) shows the usual decrease when the tip touches the surface, but it also shows an inverted peak upon tip retraction when the displacement approaches the contour length of the polymer. The amplitude then reaches the free amplitude plateau when the displacement exceeds the contour length of the polymer and the ligand detaches from the receptor. The latter transient amplitude decrease can be attributed to the fact that, when the tether extension approaches its contour length, the entropic elasticity stiffness approaches the cantilever spring constant. This causes a shift in resonant frequency and phase, and a transfer of energy to higher harmonics, all of which lead a decrease in the amplitude of the first harmonic. This effect is reproduced by simple simulations (vide infra). In addition, a significant extent

(41) (a) Ashby, P. D.; Lieber, C. M. *J. Am. Chem. Soc.* **2005**, *127*, 6814−6818. (b) Hoffmann, P. M.; Jeffery, S.; Pethica, J. B.; Ozer, H. O.; Oral, A. *Phys. Rev. Lett.* **2001**, *87*, 265502.

(42) Wong, S. S.; Joselevich, E.; Woolley, A. T.; Cheung, C. L.; Lieber, C. M. *Nature* **1998**, *394*, 52−55.

(43) Boukobza, E.; Sonnenfeld, A.; Haran, G. *J. Phys. Chem. B* **2001**, *105*, 12165−12170.

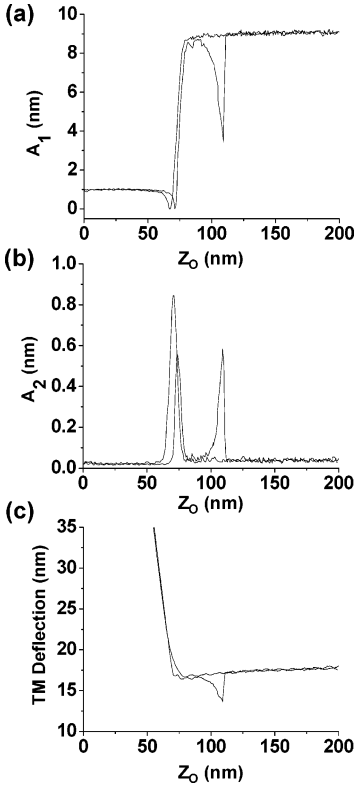

Figure 2. Fourier transformed force spectroscopy of a single polymer chain containing a ligand attached to its end, on a sample containing receptor molecules. (a) First harmonic amplitude vs distance. (b) Second harmonic amplitude vs distance. (c) Tapping-mode deflection vs distance, representing the tip average deflection filtered from oscillations.

of amplitude decrease could be due to energy dissipation by viscoelasticity, although this effect is not necessary to account for the phenomenon, as shown by the simulations.

The second harmonic amplitude (Figure 2b) shows a first peak when the tip taps the surface, as a result of VDW interactions when the tip is close to the surface, and a second peak when the displacement approaches the polymer contour length. This second peak can be attributed to the fact that the polymer elasticity becomes acutely nonlinear when its extension approaches it contour length, before the biotin end detaches from the immobilized streptavidin. The tapping mode deflection (Figure 2c) derived the DC part of the photodetector signal, and corresponding to the mean deflection filtered from oscillations, displays a typical force-displacement behavior that differs very little from force curves obtained without oscillation. Accordingly, it shows a peak corresponding to the entropic elasticity of the tether until the ligand detaches from the receptor.

Analysis of Probe Motion upon Molecular Recognition. The motion of the tip during a molecular recognition event was monitored with a data-acquisition card. Figure 3a shows that the tip motion clearly deviates from a sinusoidal shape when the tip retracts from the surface and the tip−sample distance approaches the contour length of the polymer. After ligand−receptor unbinding (Figure 3c), the tip oscillations become highly harmonic. The off-line Fourier transformations of the tip motion (Figure 3b,d) highlight the relative deviation from harmonicity upon molecular recognition, which manifests itself in the appearance of a significant peak of higher harmonics. This is consistent with the on-line evolution of the higher harmonics, shown in Figure 2b. It must be noted that the

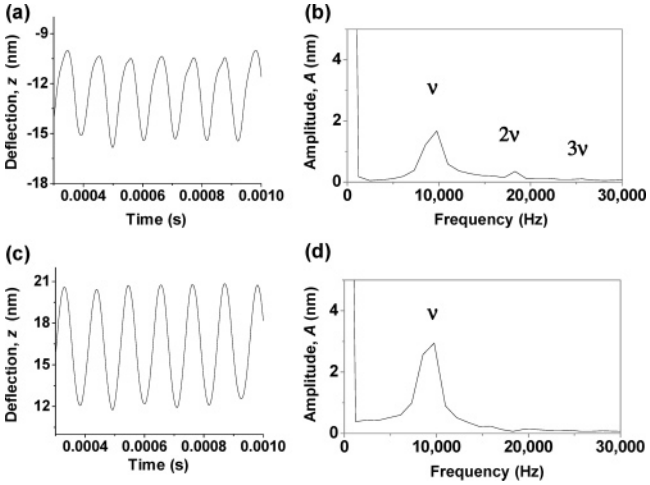

Figure 3. Motion of the biotin-PEG-functionalized probe. (a) Anharmonic motion during a molecular recognition event and (b) its Fourier transformation. (c) Harmonic motion after rupture of the ligand−receptor complex and (d) its Fourier transformation.

appearance of these higher harmonics is only seen in some of the approach−retract cycles, the frequency of the event increasing with the coverage of streptavidin molecules on the sample, and is inhibited by addition of free biotin to the solution. Moreover, the appearance of higher harmonics in a particular force measurement loop is always correlated with the observation of a decrease in the DC component. Thus, the appearance of higher harmonics constitutes a specific signature of molecular recognition.

Theoretical Simulations. The experimental results described in Figure 3 could be rationalized by means of a theoretical simulation. The equation of motion (eq 1) was numerically solved by a Runge−Kutta algorithm[46] using experimental parameters for the cantilever, tether, and ligand−receptor unbinding force, and the estimated quality factor $Q = 2$ (based on the measured Q factor from the thermal noise in liquid, $Q = 1.92 \pm 0.04$). Figure 4 shows the simulated tip motion and its Fourier transformation, for a particular *z*-piezo displacement and a peak-to-peak amplitude comparable to the contour length, with and without ligand−receptor binding. The tip motion with ligand−receptor binding (Figure 4a) exhibits a large deviation from a sine function when the tip is far from the surface, in addition to a small deviation when it approaches the surface. The upper deviation can be attributed to the nonlinearity of the polymer elasticity when the polymer extension approaches the contour length, whereas the lower deviation can be attributed to the nonlinearity of van der Waals forces between the tip and the surface within a range of a few nanometers. The simulation without the tethered ligand−receptor interaction (Figure 4c) is nearly harmonic. The relative deviations from harmonicity are highlighted by the presence or absence of higher harmonics in Fourier transformations (parts b and d, respectively, of Figure 4).

The simulated tip motion shown in Figure 4a reproduces the described features of the experimental tip motion shown in

(44) Weisstein, E. W. Runge-Kutta Methodol. From *MathWorld*, A Wolfram Web Resource. http://mathworld.wolfram.com/Runge-Kuttamethodol.html.
(45) Schroeder, C. M.; Babcock, H. P.; Shaqfeh, E. S. G.; Chu, S. *Science* **2003**, *301*, 1515−1519.
(46) Bohbot-Raviv, Y.; Zhao, W. Z.; Feingold, M.; Wiggins, C. H.; Granek, R. *Phys. Rev. Lett.* **2004**, *92*, Art. No. 098101.

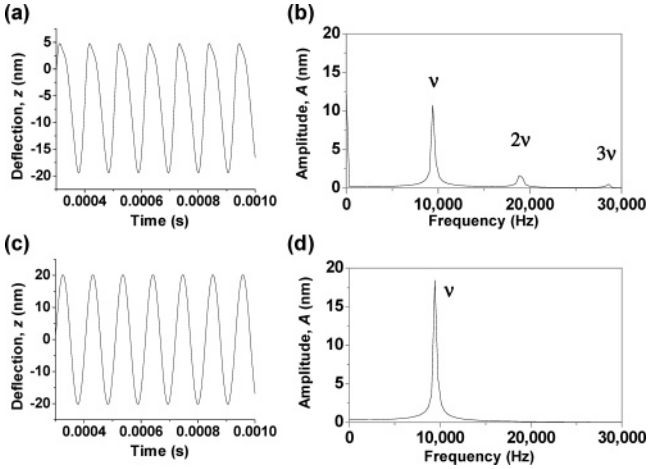

Figure 4. Theoretical simulation of the motion of the biotin-PEG-functionalized probe, analogous to the experimental date of Figure 3. (a) During a molecular recognition event and (b) its Fourier transformation. (c) Without molecular recognition and (d) its Fourier transformation.

Figure 3a, namely, a large deviation from a sine function when the tip is far from the surface, and a small deviation when it approaches the surface. However, the simulated motion shows a lack of acceleration in the downward motion shortly after maximal extension, whereas the experimental motion shows a deceleration in the upward motion shortly before maximal extension. This discrepancy is not yet clearly understood but could be due to a certain oversimplification in our model. One possible explanation is that it takes some time for the polymer to extend itself due to a viscous behavior that is neglected by the model. The dynamics of a single polymer far from equilibrium is certainly an interesting topic,[45,46] relevant to these experiments, but presently beyond the scope of our discussion.

A simulation of the Fourier transformed force spectroscopy experiments shown in Figure 2 was done by numerically solving the equation of motion as in Figure 4, but for a series of different *z*-piezo extension values. The amplitude of the selected harmonic was calculated as the square root of the area of the corresponding peak in the power spectrum. This was done for both the first and second harmonics, with and without the contribution from the polymer elasticity. The parameters were chosen for light tapping, i.e., when the setpoint amplitude is close to the free amplitude. Figure 5 shows the results of these simulations plotted as a function of *z*-piezo displacement, z_0. The simulation qualitatively reproduces the interesting phenomena observed in Figure 2. The theoretical curves without polymer describe the oscillatory behavior when the sample extends toward the tip, whereas the theoretical curves with the polymer describe the oscillatory behavior when the sample retracts after the biotin has bound to the streptavidin, until it detaches.

Higher-Harmonics Imaging of Molecular Recognition. The previous experiments established that the appearance of higher harmonics in the motion of the ligand-tethered cantilevered tip is a signature of molecular recognition that is attributed to the nonlinear entropic elasticity of the polymeric tether. Now we scan the entropic probe over the surface (scan rate 1 Hz) to obtain real-time spatially resolved images of the molecular recognition events. The peak-to-peak amplitude is comparable to the contour length of the tether (30 ± 5 nm), to enhance the entropic effect, as schematically described in Figure 1b. Parts a and b of Figure 6 show the topography and second harmonic

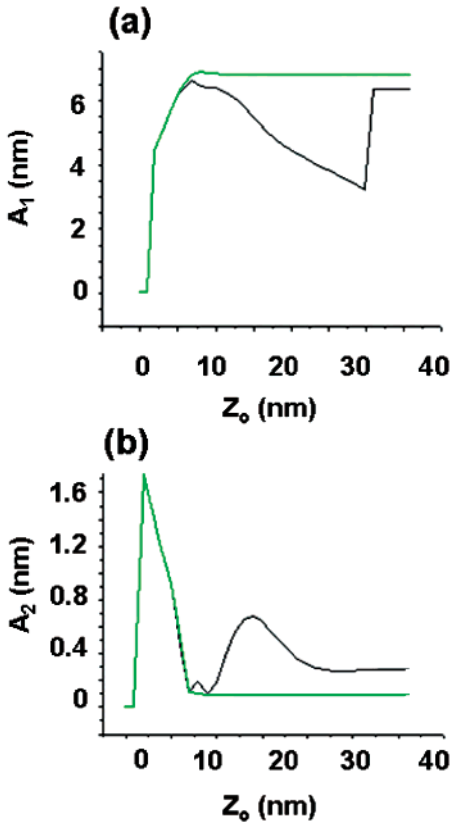

Figure 5. Simulation of the higher-harmonics force spectroscopy experiments for a PEG-biotin molecule binding streptavidin with (black) and without binding (green). (a) First-harmonic amplitude vs distance. (b) Second-harmonic amplitude vs distance.

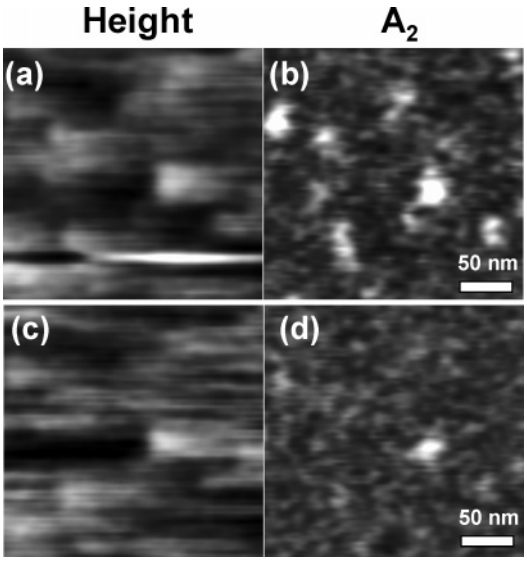

Figure 6. Molecular recognition imaging of streptavidin molecules by HH-AFM with a biotin-PEG-functionalized tip. (a) Topographic (height) image. (b) Second-harmonic amplitude image. (c) Topographic image after addition of 10 mM free biotin to solution. (d) Second-harmonic amplitude image after addition of 10 mM free biotin to solution.

amplitude signals, respectively. Parts c and d of Figures 6 display the same measurements after addition of free biotin in solution (10 mM, for 30 min), which should inhibit the binding of the tethered ligand to streptavidin. The second-harmonic amplitude image (Figure 6b) shows a series of high-contrast objects that correspond to an analogous constellation of objects in the simultaneous topographic image (Figure 6a). After

addition of free biotin to the solution, the topographic image remains nearly the same, whereas the second-harmonic amplitude image shows that almost all the high-contrast objects have disappeared. The myriad of low-contrast small objects in the background remains unchanged and can be attributed to nonspecific interactions, which are not affected by the addition of free biotin. It is interesting to note that the topographic image after inhibition (Figure 6c) still shows the objects that were seen in the second-harmonic image before inhibition but which disappeared after inhibition. This inhibition experiment demonstrates the specificity of the second-harmonic amplitude image to molecular recognition. It must be emphasized that the topographic image is not significantly modified by the inhibition of molecular recognition. This might be surprising in light of the fact that molecular recognition also affects the amplitude of the first-harmonic amplitude (as shown in Figures 2a and 5a) since the feedback system is set on the first-harmonic amplitude. This contrasts with previous observations.[32] However, in our case the peak-to-peak amplitude is set close to the contour length of the tether (Figure 1b), and not a fraction of it (Figure 1a). In these conditions, the apparent height of the streptavidin cannot be increased by the molecular recognition because, if the tip height exceeds the length of the tether, the tethered biotin detaches from the streptavidin, which increases the first-harmonic amplitude, thus prompting the feedback system to return the tip to the surface. Therefore, having set the feedback on a peak-to-peak amplitude near the contour length of the tether not only enhances the entropic effect but also forces the tip to keep tapping on the surface and the molecules bound to it, and thus keep reporting the topography. Under these circumstances, the deviation from harmonic oscillation can be due to the nonlinearity of both the interaction with the surface (as the left peak in Figures 2b and 5b, and as the minima in Figures 3a and 4a) and the nonlinearity of the entropic elasticity of the tether near full extension (as the right peak in Figures 2b and 5b, and the maxima in Figures 3a and 4a). Of the two nonlinear interactions, the one with the surface is relatively invariant of position, whereas the entropic elasticity varies significantly upon molecular recognition. Therefore, the contrast in second-harmonic amplitude is specifically related to molecular recognition.

Characterization of the Specific Probing Mechanism. Further evidence for the mechanism of specific probing of molecular recognition is obtained from studying the dependence of second-harmonic amplitude contrast on peak-to-peak amplitude. Figure 7 shows simultaneous topographic and second-harmonic amplitude images of the same immobilized streptavidin with a biotin-PEG-tip probe at peak-to-peak amplitudes lower than (10 ± 2 nm and 20 ± 3 nm), comparable to (30 ± 5 nm), and higher than (40 ± 6 nm to 70 ± 10 nm) the contour length of the PEG tether (30 ± 5 nm).[47] The topographic images with increasing amplitude are slightly sharper but not significantly different. However, the second-harmonic amplitude images show a contrast that increases as the peak-to-peak amplitude approaches the contour length of the tether and decreases when the amplitude exceeds the contour length. This is clearly seen in the detailed zoom for one high-contrast object, while the contrast dependence on amplitude is shown in Figure 7f. This effect can be attributed to the fact that the entropic elasticity increases toward full extension, beyond which ligand–receptor unbinding occurs, as schematically represented by

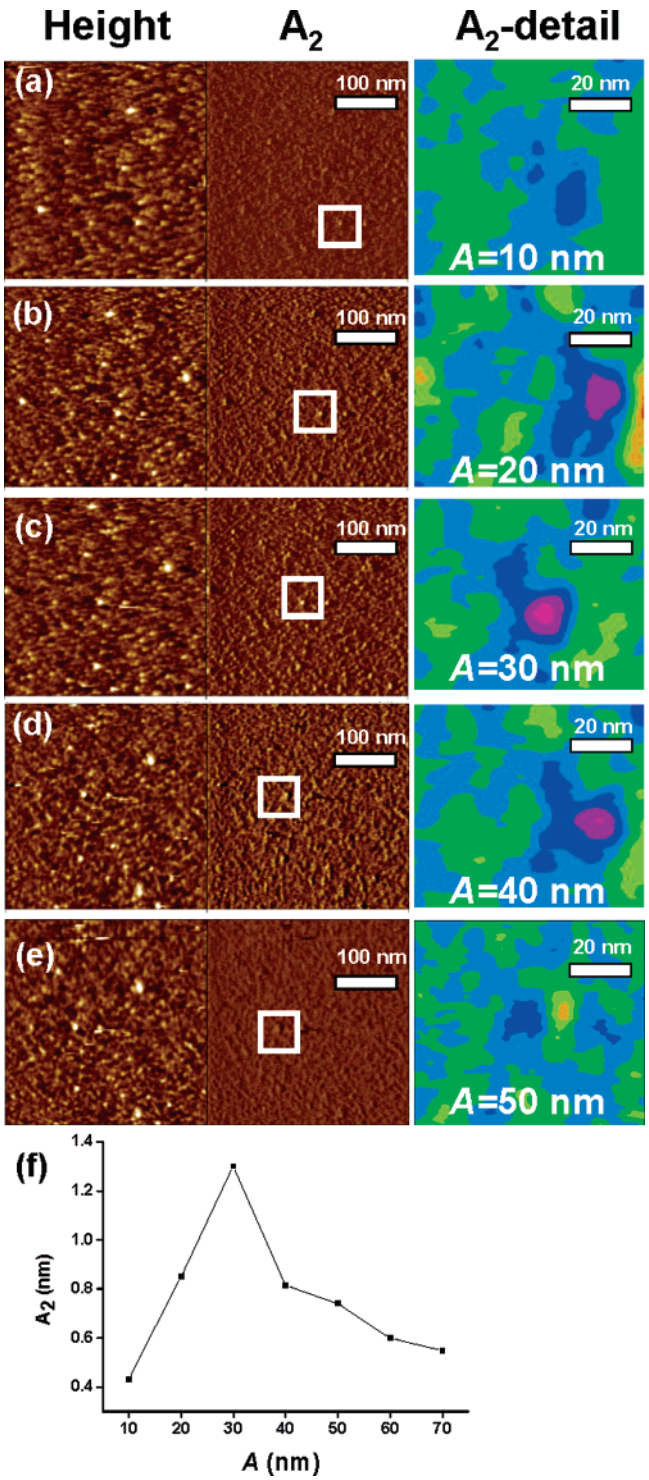

Figure 7. Effect of amplitude on the molecular recognition microscopy. The peak-to-peak amplitude is changed to be smaller than, comparable to, or larger than the contour length ($L = 30 \pm 5$ nm). (a) $A = 10 \pm 2$ nm. (b) $A = 20 \pm 3$ nm. (c) $A = 30 \pm 5$ nm. (d) $A = 40 \pm 6$ nm. (e) $A = 50 \pm 7$ nm. (f) Contrast dependence of A_2 with A. The left column displays the topography images, the center column shows second-harmonic amplitude images, and the right column shows a detail of the latter for a specific object, whose contrast varies with the changes in peak-to-peak amplitude. The drive amplitude was also increased to keep the setpoint amplitude close to the free amplitude and, hence, to minimize the nonspecific anharmonicity that arises from the repulsive tip–sample interactions.

(47) A ca. 15% error range in the amplitude stems mainly from the variation in the determination of the photodetector sensitivity, whereas the error range in the contour length is due to the polydispersity of the PEG polymer length.

Figure 1. Additional evidence is obtained when this experiment is done with probes having several tethered biotin molecules at different positions (Supporting Information).

Operative Range and Limitations. A significant aspect that must be addressed is that the dwell time of the tethered ligand near the receptor is longer than the *on* time of ligand−receptor binding. The *on* time for ligand−receptor binding τ_{on} is given, as written[32] in eq 6, by the second-order rate constant of binding k_{on} and the local concentration c of the ligand in the reach volume allowed by the tether and the cantilever oscillation. This concentration, as given by eq 7, corresponds to the number of moles for one molecule (i.e. the reciprocal of Avogadro's number N_A) divided by the volume of a cylinder whose height is the peak-to-peak amplitude A, and its radius is the tether contour length L. According to data found in the literature,[48] $k_{on} = 5 \times 10^6$ $M^{-1}s^{-1}$. Since the binding process is not diffusion-controlled, we can neglect the effect of the tether on the kinetic constant. The dwell time τ_D of the ligand in this reach volume allowed by the tether is given, as written in eq 8, by the tip velocity v and the contour length of the tether.

$$\tau_{on} = \frac{1}{ck_{on}} \tag{6}$$

$$c = \frac{1}{N_A \pi L^2 A} \tag{7}$$

$$\tau_D = \frac{2L}{v} \tag{8}$$

Using the experimental parameters $L = 30$ nm, $A = 30$ nm, and $v = 1-2$ μm/s, we calculate that $\tau_{on} = 10$ ms, and $\tau_D = 60-120$ ms. Since the *on* time required for ligand−receptor binding is 1 order of magnitude longer than the time dwelt by the ligand at a reachable distance, it is ensured that molecular recognition has enough time to take place, as long as the peak-to-peak amplitude is not larger than the polymer contour length (as schematically shown in Figure 1a,b). However, if the amplitude exceeds the contour length (Figure 1c), then the receptor escapes from the reach volume, and the dwell time becomes shorter than the period of the oscillation, $\tau_D < (8\ \text{kHz})^{-1} = 125$ μs, which is significantly shorter than the on time ($\tau_{on} = 10$ ms). This explains why the second-harmonic amplitude has a resonant amplitude of maximum contrast near the contour length, as shown in Figure 7. Following this analysis, it should be emphasized that the anharmonicity is not caused by binding−unbinding events, which are much slower than the oscillation period, but by the nonlinear behavior of the polymer chain.

The existence of a resonant amplitude that leads to a maximum in the contrast of the second-harmonic signal, and which is specific to the length of the tether, is of particular interest because it can be exploited to enhance the specificity of this mode of molecular recognition imaging against nonspecific interactions, which might also be nonlinear (e.g., electrostatic, van der Waals, etc), but have no specific resonant amplitude. This represents a significant advantage with respect to other techniques. From a practical point of view, higher-harmonics AFM does not require any special electronics, except for a lock-in-amplifier with harmonic analysis, which is a very common, commercially available electronic instrument. The spatial resolution of our imaging is limited by the length of the tether to $2L = 60$ nm and is consistent with the observed images (Figures 6 and 7). The efficiency of the technique is limited by the maximal tip velocity required to keep the dwell time longer than the *on* time $\tau_D < \tau_{on}$. Assuming that $A \approx L$, the maximal tip velocity is given by eq 9. Thus, using shorter tethers should increase the resolution and the efficiency of the molecular recognition imaging for a particular ligand−receptor pair.

$$v_{max} = \frac{\pi L^2 N_A}{2k_{on}} \tag{9}$$

Conclusions

Detection and mapping of single-molecule recognition by AFM simultaneous and independent of topographic imaging has been achieved using tips modified with a polymer-tether ligand, and analyzing in real time the amplitude of higher harmonics in the cantilever motion. The single polymer chain specifically transduces the decrease in the translational and rotational entropy of the ligand upon binding the receptor, into a measurable force. This is an interesting example of a single-molecule mechanical device that functions as a chemical and biological sensor. The optimal conditions for a specific probe to be operative is that the entropic elasticity of the tether must be comparable to the unbinding stiffness of the ligand−receptor complex. Since the entropic elasticity is nonlinear and varies over a significant range, limited by the segment elasticity, it can be predicted that a flexible, water-soluble polymer, such as poly(ethylene glycol), can be suitable for the specific detection and mapping of a wide range of ligand−receptor pairs. We can thus envisage that this mechanism of entropic elasticity-based probing can be adopted as a general approach for the detection and imaging of molecular recognition interactions in a variety of interesting systems, such as sequence-specific imaging of DNA, immunospecific imaging of biological membranes, and many more.

Acknowledgment. This research has been supported by the Israel Science Foundation, the Djanogly Center for New Scientists, the Ilse Katz Institute for Material Sciences and Magnetic Resonance Research, the Hellen and Martin Kimmel Center for Nanoscale Science, the Philip M. Klutznick Fund for Research, Alhadeff Research Award, and Legrain Research Award. E.J. is incumbent of the Victor Erlich development chair.

Supporting Information Available: Force-distance curves and probe selection procedure, additional data for the characterization of the specific probing mechanism. This material is available free of charge via the Internet at http://pubs.acs.org.

JA051642V

(48) Qureshi, M. H.; Yeung, J. C.; Wu, S. C.; Wong, S. L. *J. Biol. Chem.* **2001**, *276*, 46422−46428.